Macromolecules

pubs.acs.org/Macromolecules Article

# Depletion Interaction between Cylindrical Inclusions in Polymer Brushes

Ji Woong Yu, Daeseong Yong, Bae-Yeun Ha,* and Changbong Hyeon*

Cite This: *Macromolecules* 2025, 58, 8099−8106 Read Online

ACCESS | Metrics & More | Article Recommendations | Supporting Information

**ABSTRACT:** Inclusions in mobile brushes experience apparent (depletion) attraction, which arises from the tendency to minimize the volume of depletion zones around the inclusions, thereby maximizing the entropy of the surrounding polymers. Here, we study the brush-induced depletion attraction between cylindrical inclusions using molecular dynamics simulations and the Asakura-Oosawa theory. Our considerations find that the correlation blobs defined in the brush environment serve as the fundamental units of the attraction. In tall brushes, however, the entropy of the overgrown polymer competes with the depletion attraction between the inclusions. As a result, the brush-induced depletion interaction displays nonmonotonic variations with the brush height. Our study not only expands the repertoire of colloid−polymer mixtures to depletion interactions in brushes but also suggests the brush-induced depletion interaction as a previously unappreciated mechanism for glycocalyx-induced protein cluster formation on cell surfaces.

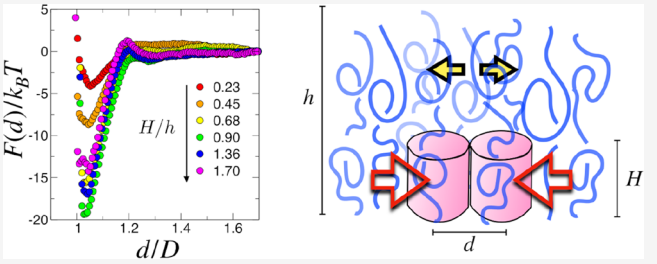




Protein clusters are ubiquitous in cell membranes, and their cellular functions have been a subject of great interest.[1−5] For example, an oligomerized form of microbial rhodopsins functions as a light-driven ion-pump or ion-channel in the native membrane.[6−10] It has been shown that the glycocalyx, a layer of glycolipids and glycoproteins that densely coat the cell surface, plays vital roles in cell−cell adhesion, communication, and signaling by promoting the integrin nanocluster formation[11−14] and regulates the cancer cell progression.[15] Polymer brush-induced depletion attraction has recently been suggested as one of the key driving forces for the transmembrane protein clustering in biological membranes,[16,17] among other mechanisms, such as membrane undulation-induced thermal Casimir forces,[18−21] protein−protein interaction,[22−25] and membrane curvature-mediated interaction.[26,27]

The attraction between inclusions in a suspension of nonadsorbing depletants characterized with purely repulsive interaction is entropic in nature, arising from an osmotic imbalance of depletants near the depletion layers.[28,29] Although the Asakura-Oosawa (AO) theory was originally proposed for interactions between hard spheres or flat surfaces suspended in a solution of depletants in three dimensions, it can straightforwardly be extended to other geometry or polymeric systems as well as to those in two dimensions (2D).[30−33] For extensively studied systems of colloid−polymer mixtures,[28−31,34−45] the gyration radius of polymers ($R_g$) and the radius of colloidal particles ($R_c$) serve as the two primary length scales. Depending on their size ratio, $q = R_g/R_c$, the depletion interactions are either in the *colloid* ($q < 1$)[46] or in the *protein limit* ($q > 1$).[42,47,48] For our cylinder-brush system, on the other hand, where the cylinders can be deemed effectively in a semidilute polymer solution of correlation length $\xi$, $q_c = \xi/D$, in which $R_g$ and $R_c$ in $q$ are replaced with the correlation length $\xi$ and the cylinder diameter $D$, respectively, becomes a relevant parameter. Together with $q_c$, due to the presence of another length scale set by the brush height ($H$) relative to the inclusion height ($h$), i.e., $H/h$, the brush-induced depletion interactions are formally categorized into four distinct regimes (Figure 1).

Here, we first review the basics of brush polymers and revisit a quasi-2D version of the AO theory for the brush-induced depletion interaction.[16] The AO theory is employed to account for the potentials of mean force (PMFs) calculated from molecular dynamics (MD) simulations under varying brush heights and grafting densities. We not only highlight the efficacy of the blob concept[49] in quantitative understanding of depletion interactions in a brush environment, but also demonstrate that the varying brush height introduces additional complexity to the problem. Our study sheds light on membrane biophysics associated with protein nanocluster formation in glycocalyx.[11−15]

**Received:** December 10, 2024
**Revised:** May 28, 2025
**Accepted:** July 22, 2025
**Published:** July 29, 2025

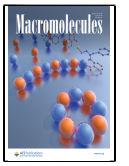





https://doi.org/10.1021/acs.macromol.4c03070
*Macromolecules* 2025, 58, 8099−8106

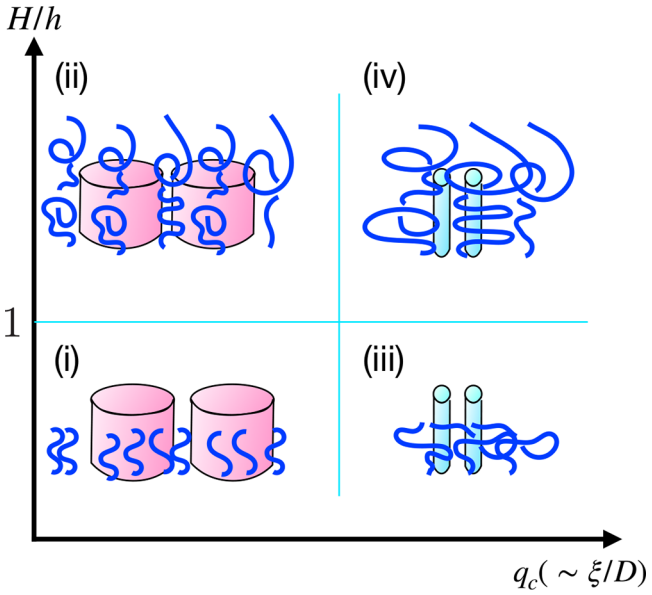


**Figure 1.** Four distinct regimes of brush-induced depletion interactions between cylindrical inclusions. (i) $H/h < 1$, $q_c < 1$; (ii) $H/h > 1$, $q_c < 1$; (iii) $H/h < 1$, $q_c > 1$; (iv) $H/h > 1$, $q_c > 1$.

## POLYMER BRUSH

We consider a polymer brush where $n_p$ polymers, each consisting of $N$ segments, are end-grafted to a 2D surface of area $A$ but laterally mobile on the grafting surface. When the grafting density, $\sigma = n_p/A$, is greater than that defined by the Flory radius of an isolated chain ($R_F \simeq bN^{3/5}$), i.e., $\sigma > R_F^{-2}$, the polymer chains overlap with each other and transition from a mushroom-like configuration to a string of $N/g$ *correlated* blobs of size each $\xi$ ($\simeq \tau^{1/5} b g^{3/5}$), forming a brush of height ($H$) that satisfies the Alexander-de Gennes brush scaling,[50−52] $H \simeq (N/g)\xi \simeq Nb(\tau\sigma b^2)^{1/3}$. Here, $\tau(=(T-\Theta)/T \sim O(1))$ is the relative temperature difference from the theta temperature ($\Theta$) and associated with the second virial coefficient $B_2 \sim \tau b^3$, which we set $\tau = 1$ for convenience in this paper, and $\sigma$ is related to $\xi$ as $\sigma \simeq 1/\xi^2$.

The interior of a brush ($\xi < z < H$) is effectively in the semidilute regime packed with correlation blobs of size $\xi$ which changes with the monomer volume fraction ($\phi \simeq g/\xi^3$) as $\xi \simeq b\phi^{-\gamma}$ with $\gamma = \nu/(3\nu - 1) \approx 3/4$ for $\nu = 3/5$.[49] Thus, the osmotic pressure inside the brush is expected to follow the des Cloizeaux scaling, $\Pi/k_BT \sim 1/\xi^3 \sim \phi^{9/4}/b^3 \sim (\sigma b^2)^{3/2}$,[49,53] where $k_B$ is the Boltzmann constant.

## AO THEORY FOR BRUSH-INDUCED DEPLETION INTERACTION

For a brush system that contains two parallelly aligned cylindrical inclusions, mimicking signaling transmembrane receptor proteins, e.g., integrins, separated by a center-to-center distance $d$, the total volume accessible for brush polymers increases as the inclusions are brought together from $V(d) = V_>$ for $d > D + 2\delta_c$ to $V(d) = V_> + V_{ex}(d)$ for $D \le d \le D + 2\delta_c$, where $V_> = (A - \pi D^2/2) \times \min(h, H) \approx A \times \min(h, H)$, $\delta_c$ denotes the depletion layer thickness, and $V_{ex}(d) > 0$. Then, according to the AO theory, the effective interaction between these inclusions arises from the tendency to minimize the volume of depletion zones, which in turn maximizes the accessible volume for brush polymers to explore. Thus, the AO potential is given by

$$\begin{aligned}\beta F_{AO}(d;\delta_c) &\simeq -n_p\left(\frac{\min(h,H)}{\xi}\right)\log\left[1+\frac{V_{ex}(d;\delta_c)}{V_>}\right]\\ &\approx -\frac{\sigma}{\xi}V_{ex}(d;\delta_c),\end{aligned} \quad (1)$$

where $\beta = 1/k_BT$. Here, it is conjectured that each correlation blob contributes a free energy of $\sim O(1)k_BT$ to the depletion interaction. Thus, $n_p \times \min(h, H)/\xi$ amounts to the number of blobs in the system characterized by the volume of $A\min(h, H)$. The second line of eq 1 is obtained from $V_{ex}/V_> \ll 1$ with $\sigma = n_p/A$. Our incorporation of the blob idea[49] into the AO theory will be justified through analysis of the numerical results of brush-induced depletion interaction.

In eq 1, the excess volume for brush polymers is equivalent to the excess area $A_{ex}(d;\delta_c)$ multiplied by the height of either

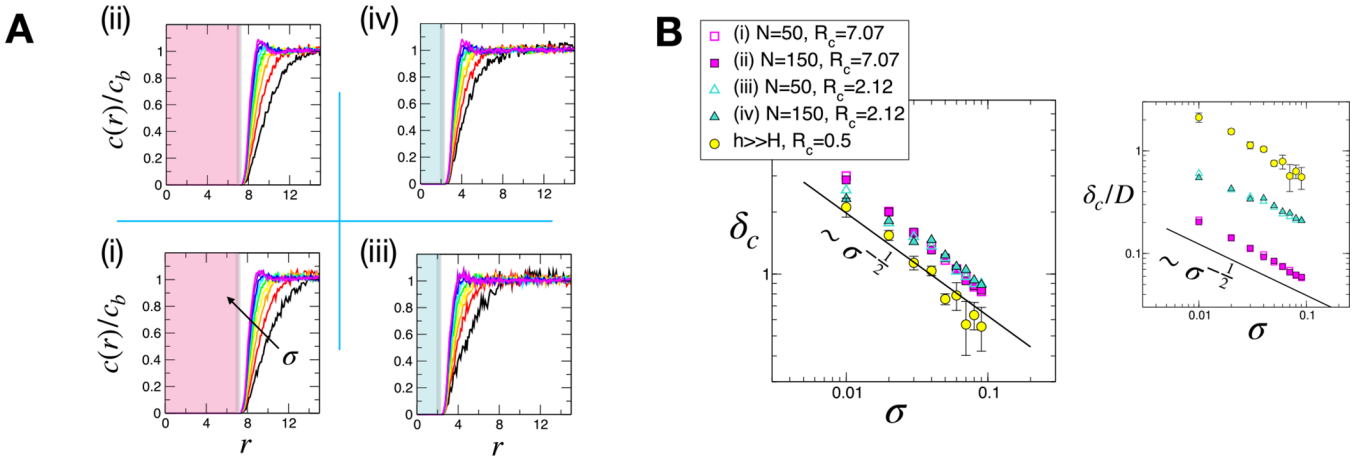


**Figure 2.** (A) Monomer concentrations around a cylindrical inclusion with $R_c/b = 7.07$ (pink box) $R_c/b = 2.12$ (pale blue box) obtained from MD simulations in four distinct cases illustrated in Figure 1. (B) Depletion layer thickness ($\delta_c$) against grafting density ($\sigma$) for the four regimes (i−iv), and those calculated around a needle-like inclusion (yellow circles; a cylinder with $R_c/b = 0.5$ and $h \gg H$). The line of $\delta_c \sim \sigma^{-1/2}$ is depicted as a reference. (Inset) Plot of depletion layer thickness rescaled by the cylinder diameter ($\delta_c/D$) against $\sigma$.



https://doi.org/10.1021/acs.macromol.4c03070
Macromolecules 2025, 58, 8099−8106

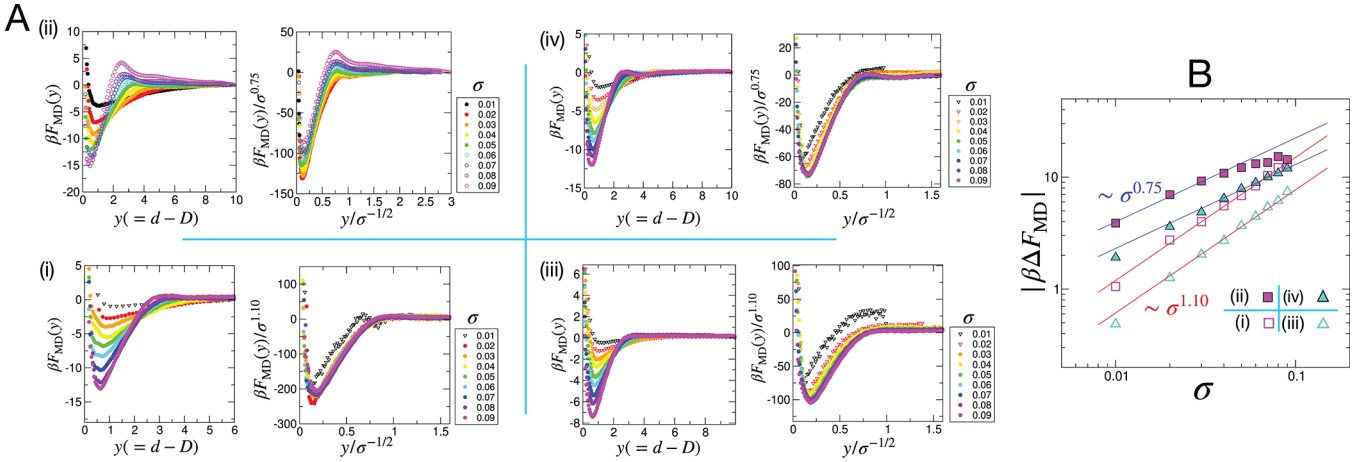


**Figure 3.** PMFs between cylinders with varying $\sigma$ obtained from MD simulations for the four distinct regimes (i)−(iv). (A) (left) PMFs versus $y = d - D$. (right) PMFs in the range of $\sigma$ represented by the filled circles are collapsed onto one another when the distance and free energy are rescaled, respectively, with $\sigma^{-1/2}(=\xi)$ and $\sigma^{\alpha}$ ($\alpha = 1.10$ for $H/h < 1$ in (i) and (iii); $\alpha = 0.75$ for $H/h > 1$ in (ii) and (iv)). (B) $|\beta\Delta F_{MD}|$ versus $\sigma$. The red and blue lines depict the scalings of $\sim\sigma^{1.10}$ and $\sim\sigma^{0.75}$, respectively.

brush ($H$) or inclusion ($h$), whichever is smaller, i.e., $V_{ex}(d;\delta_c) = A_{ex}(d;\delta_c)\min(h, H)$ with

$$A_{ex}(x;\lambda_c) = \frac{D^2}{2}\left[(1+\lambda_c)^2\cos^{-1}\left(\frac{x}{1+\lambda_c}\right) - x^2\sqrt{\left(\frac{1+\lambda_c}{x}\right)^2 - 1}\right] \quad (2)$$

where we used the rescaled distance $x = d/D$ and thickness $\lambda_c = \delta_c/D$ ($1 \le x \le 1 + \lambda_c$) (see SI for the details of derivation). Thus, the AO potential at $x$ reads

$$\beta F_{AO}(x) \approx -\sigma\left(\frac{\min(h, H)}{\xi}\right)A_{ex}(x;\lambda_c) \quad (3)$$

In fact, an identical expression can be derived by considering the free energy gain due to the excess volume of $\min(h, H)A_{ex}$ created in a semidilute solution whose osmotic pressure is given by $\beta\Pi \sim 1/\xi^3$,

$$\beta F_{AO}(x) \approx -\beta\Pi \times \min(h, H)A_{ex}(x;\lambda_c) \quad (4)$$

## DEPLETION LAYER THICKNESS

To evaluate eqs 3 or 4, it is necessary to know the depletion layer thickness ($\delta_c$) associated with the parameter $\lambda_c$ in $A_{ex}(x;\lambda_c)$ (eq 2). For spheres of radius $R_c$ each in a semidilute polymer solution, it is known that $\delta_c \sim \xi$ for the limit $\xi \ll R_c$,[30,35] whereas for the opposite limit $\xi \gg R_c$, $\delta_c$ is constant as $\delta_c \sim R_c$,[47,54,55] independent of depletant (polymer) concentration. What remains to be clarified is the thickness of a depletion layer around a cylindrical object in a polymer brush or a semidilute polymer solution. Of particular interest is the case of $R_c < \xi < h$. At first glance, it appears that $\delta_c$ in this case would combine the features of the two limiting cases for spherical inclusions discussed above.

For our cylinder-brush system, we calculate $\delta_c$ explicitly from the concentration profiles around a cylinder of radius $R_c$ ($= D/2$) (Figure 2) through the relation[43]

$$\pi(R_c + \delta_c)^2 = \pi R_c^2 + \int_{R_c}^{\infty} 2\pi r(1 - c(r)/c_b)dr \quad (5)$$

where $c(r)/c_b$ is the concentration profile of monomers normalized by the bulk concentration ($c_b \equiv c$ ($r > \xi$)) that is reached at a distance of the order of the correlation blob size.[35] For polymers grafted as in brushes, the symmetry along the brush height is broken; however, the brush height-dependence of the concentration profile around the cylinder is found insignificant. The calculations for $\delta_c$ are carried out over the range of $\sigma b^2$ ($= 0.01 - 0.09$) and $D/b = 1, 3\sqrt{2}$ and $10\sqrt{2}$, so that the parameter $q_c = \xi/D \simeq \delta_c/D \simeq (\sigma^{1/2}D)^{-1}$ encompasses the range of $q_{c,min} < q_c < q_{c,max}$ with $q_{c,min} \simeq 0.235$ for $\sigma b^2 = 0.09$ and $D/b = 10\sqrt{2}$ and $q_{c,max} \simeq 10.0$ for $\sigma b^2 = 0.01$ and $D/b = 1$ (Figure 2). Throughout the paper, all lengths are measured in units of $b$, unless otherwise stated.

First, our explicit calculation using MD simulation results finds that the depletion layer thickness is narrow compared to the diameter of the cylinder ($\delta_c/D < 1$) over the whole range of $q_c$ being explored ($0.235 \le q_c \le 10.0$). Although the depletion layer thickness around the cylinder is curvature-dependent, such that smaller cylinder curvatures lead to greater $\delta_c$'s, the actual difference between $\delta_c$'s for different $D$ is only minor (see Figure 2). Furthermore, the difference between $\delta_c$'s for the short ($H < h$) and tall brushes ($H > h$) is not statistically significant either (Figure 2B).

Second, it may be tempting to associate the $q_c > 1$ limit of cylindrical inclusions with the small-$R_c$ limit of *spherical* inclusions, where the depletion layer thickness is set by $R_c$, independent of $\xi$.[47,54,55] However, the scaling relation of $\delta_c \sim \sigma^{-1/2}$ revealed from our calculation (Figure 2B) is apparently at odds with such a notion. This signifies that the depletion layer thickness around cylindrical inclusion in brushes is dictated by the blob size ($\delta_c \sim \xi$) regardless of the value of $q_c$ (Figure 2) and that the correlation blob is the fundamental interaction unit for the brush-induced depletion attraction, which should hold for $h > \xi$. Note that the cylinder-brush system is distinguished from the colloid−polymer mixtures in that the axial dimension of cylinder ($h$) is still greater than $\xi$ (see below for additional details).


https://doi.org/10.1021/acs.macromol.4c03070
Macromolecules 2025, 58, 8099−8106

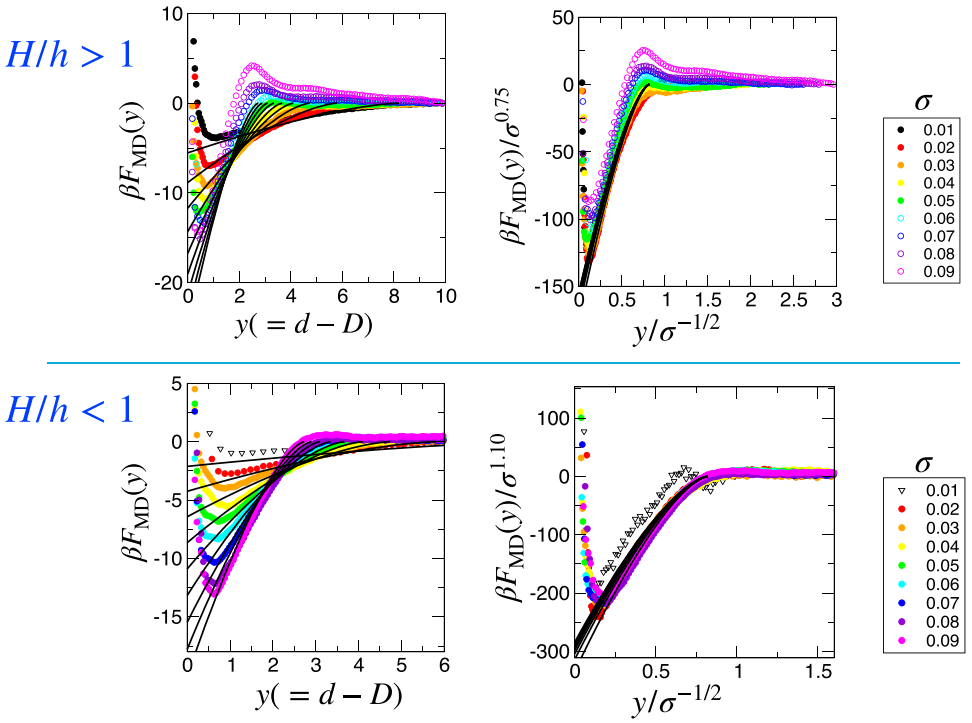


**Figure 4.** AO potentials, $\beta F_{AO}(y)$ (eq 3 with eq 2, black lines) with $D/b = 10\sqrt{2}$ and $h/b = 20\sqrt{2}$ for $N = 150$ ($H/h > 1$, top) and $N = 50$ ($H/h < 1$, bottom) after rescaling $y \rightarrow \tilde{y} \simeq y/1.22$ and $\beta F_{AO}(y) \rightarrow \beta \tilde{F}_{AO}(\tilde{y}) \simeq 1.43 \times \beta F_{AO}(\tilde{y})$ over all $\sigma$'s, where the numerical prefactors 1/1.22 and 1.43 stem from the scaling relation without prefactor ($\xi \sim \sigma^{-1/2}$) used in deriving the $\sigma$-dependent scaling of AO potentials. The $\beta \tilde{F}_{AO}(\tilde{y})$ for varying $\sigma$'s are overlaid on top of PMFs obtained from MD simulations ($\beta F_{MD}(y)$). The panels on the right show the collapsed AO potentials after rescaling $\tilde{y} \rightarrow \tilde{y}/\sigma^{-1/2}$ and $\beta \tilde{F}_{AO}(\tilde{y}) \rightarrow \beta \tilde{F}_{AO}(\tilde{y})/\sigma^{\alpha}$ with $\alpha = 1.10$ ($H/h < 1$) and $\alpha = 3/4$ ($H/h > 1$).

## ■ ANALYSIS OF PMFS FROM MD SIMULATIONS

The PMFs calculated from MD simulations for the four regimes illustrated in Figure 1 are analyzed by using eq 3 (see Figure 3). For $H < h$, $\min(h, H)/\xi = H/\xi = N/g$, and eq 2 at $x = 1$ for $\lambda_c \ll 1$ is approximated as $A_{ex}(1;\lambda_c) \sim D^2\lambda_c^{3/2} \sim D^{1/2}\delta_c^{3/2}$. From the relation of $\delta_c \sim \sigma^{-1/2}$ (Figure 2) and the blob concept with $\nu = 0.588$, the free energy gain, $\beta F_{AO}(x = 1) \equiv \beta \Delta F_{AO}$ (eq 3), is expected to scale with $\sigma$ as

$$|\beta \Delta F_{AO}| \sim \sigma \left(\frac{N}{g}\right) D^{1/2}\delta_c^{3/2} \sim N D^{1/2}\sigma^{1/4+1/2\nu} \sim \sigma^{1.10} \tag{6}$$

Figure 3B shows that the dependence of stability on $\sigma$ predicted by eq 6 well accounts for the MD simulation results. In addition, upon rescaling the inclusion gap ($y = d - D$) by the blob size ($\xi \sim \sigma^{-1/2}$) and the free energy by the $\sigma$-dependent stability (eq 6), the rescaled free energy profiles with varying $\sigma$ overlap nicely with each other (see Figure 3A-(i) and (iii)), except for those with small $\sigma$ (the empty symbols, $\sigma = 0.01$ in Figure 3A-(i) and $\sigma = 0.01$, 0.02 in Figure 3A-(iii)) which are on the border of the brush forming regime ($\sigma R_F^2 \gtrsim 1$). On the other hand, for $H > h$, the free energy gain is characterized by a distinct exponent, 3/4, as follows:

$$|\beta \Delta F_{AO}| \sim \frac{1}{\xi^3} \times h D^{1/2}\delta_c^{3/2} \sim h D^{1/2}\xi^{-3/2} \sim \sigma^{3/4} \tag{7}$$

Upon rescaling the intercylinder gap ($d - D$) by the $\sigma$-dependent blob size, and the free energy by the $\sigma$-dependent stability of the AO potential, i.e.,

$$\begin{aligned} (d - D) &\rightarrow (d - D)/\xi \sim (d - D)/\sigma^{-1/2} \\ \beta F_{MD}(y) &\rightarrow \beta F_{MD}(y)/|\beta \Delta F_{AO}| \sim \beta F_{MD}(y)/\sigma^{\alpha} \end{aligned} \tag{8}$$

where $\alpha = 1.10$ for $H < h$ and $\alpha = 3/4$ for $H > h$, the free energy profiles generated at different $\sigma$ collapse onto each other (see Figure 3A). Furthermore, Figure 4 shows that the AO potentials (eq 3) calculated using the explicit expression of $A_{ex}(x)$ (eq 2) are nicely overlaid, at least, onto the lower part of the PMFs from MD simulations, i.e., $\beta F_{MD}(y) < 0$. The repulsive barriers that appear in $\beta F_{MD}(y) > 0$ at large $\sigma$'s in Figure 3A are the most pronounced at short intercylinder separation ($y \approx (2 - 3)$ or $y/\sigma^{-1/2} \approx 0.75$) for the case of thick cylinders in tall brushes (compare the case (ii) with others in Figure 3A). The repulsive barriers in $\beta F_{MD}(y)$'s can be attributed to the formation of depletion zones above the inclusion, which will be discussed further in the section that follows. The collapse of PMFs upon the rescaling in Figure 3A, the $\sigma$-dependent scaling of the free energy gain quantitatively confirmed in Figure 3B, and the quantitative agreement between the AO potential and PMFs from MD for varying $\sigma$'s highlighted in Figure 4 lends support to our analysis based on the AO theory.

The depletion potentials and stabilities for brushes spanning from $H < h$ to $H > h$ are calculated for a fixed $\sigma$ as well (Figure 5). As predicted by the AO theory (eq 6), a cluster of inclusions is further stabilized with an increasing brush height $H$ (or $N$) as long as $H < h$. For $H > h$, however, reduction of the stability is significant ($H/h \gtrsim 1.5$), especially for the inclusions with large $R_c$ (= 7.07) (Figure 5B), which is no longer explicit in eq 7 although it correctly captures the $\sigma$-scaling.



https://doi.org/10.1021/acs.macromol.4c03070
Macromolecules 2025, 58, 8099−8106

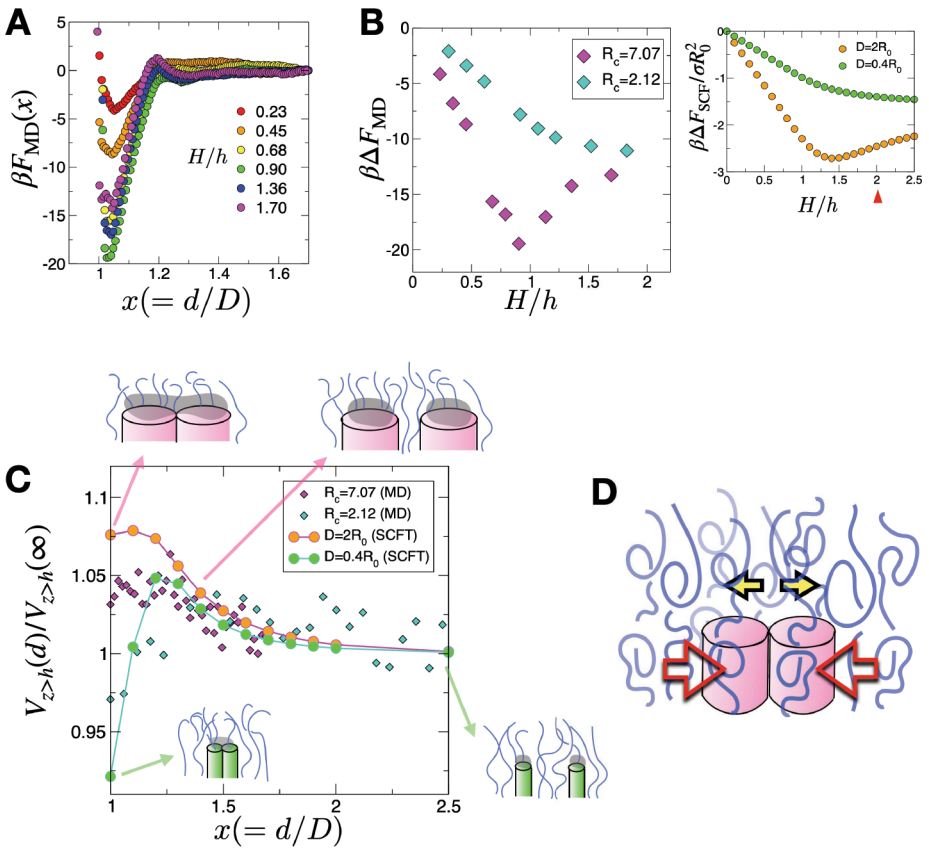


**Figure 5.** (A) PMFs from MD simulations for $R_c/b = 7.07$ at $\sigma b^2 = 0.08$ with varying $H/h$. (B) Stabilities of two cylinders as a function of $H/h$ for $R_c = 7.07$ and 2.12 at $\sigma b^2 = 0.08$. (Inset) Self-consistent field (SCF) calculations for the diameters, $D = 2R_0$ and $0.4R_0$, with the excluded volume parameter $\Lambda = 2\pi^2$ (see SI). (C) The depletion zone volume above the cylinders with increasing distance between the cylinders, $V_{z>h}(d)/V_{z>h}(\infty)$, obtained from both MD simulations (diamonds) and SCF calculations (circles) at $H/h = 2$. The volume, $V_{z>h}(d)$, is obtained by integrating the $z$-dependent volume fraction of monomers at the bulk ($\phi_b(z)$) subtracted by that at $\mathbf{r}$ over the space ($\phi(\mathbf{r};d)$), i.e., $V_{z>h}(d) = \int[\phi_b(z) - \phi(\mathbf{r};d)]d\mathbf{r}$. The cartoons depict the depletion zone volume (gray) above the thick and thin cylinders. (D) An illustration of depletion attraction (red arrows) and repulsion (yellow arrows) between two thick cylinders in tall brushes.

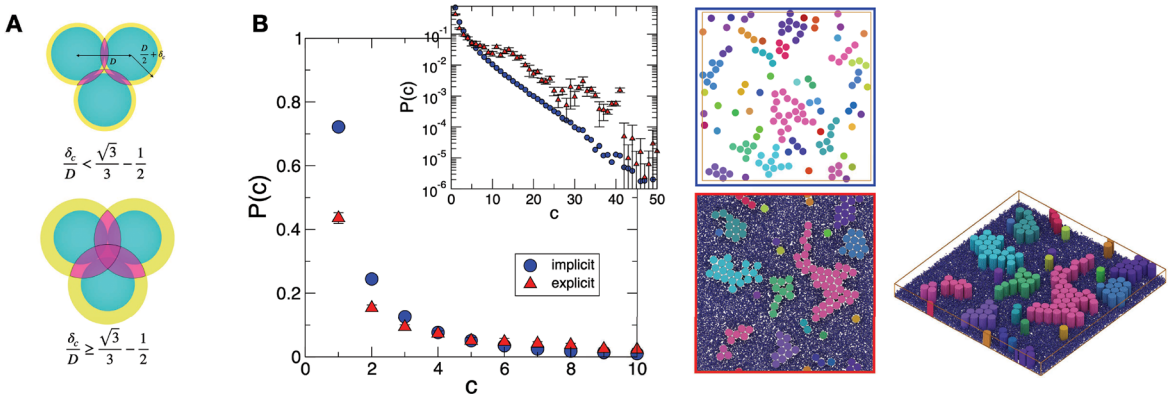


**Figure 6.** Cluster size distribution, $P(c)$, (i) based on MD PMF between two cylinders (implicit) and (ii) obtained directly from MD simulations (explicit) for cylinders with an area fraction $\phi_c = 0.2$ in brushes ($N = 20$) at $\sigma b^2 = 0.06$. For cylinders, we have chosen $D = 7.07 \times 2b$ and $h \simeq 28b$. (A) Depletion zone shared between three cylindrical inclusions under the condition of compact packing (magenta) for $\delta_c/D < \sqrt{3}/3 - 1/2$ (top) and $\delta_c/D \geq \sqrt{3}/3 - 1/2$ (bottom). (B) The plot of cluster size distribution $P(c)$ and the snapshots of clusters obtained from the implicit (top) and explicit simulations of cylinders in brushes (bottom), clarifying their similarities and differences.

Calculations of stability between cylinders in brushes based on the self-consistent field approach, $\beta\Delta F_{SCF}/\sigma R_0^2$, where $R_0^2 = Nb^2$ (see SI), confirms a similar trend of nonmonotonic variation (the inset of Figure 5B), validating its thermodynamic origin ruling out a kinetic effect. Our inspection of the results from both SCF calculation and MD simulations focusing on the depletion zone (the volume inaccessible to the polymer segments) *above* the cylinders ($V_{z>h}$, depicted in gray in the cartoons of Figure 5C) indicates that the reduction of the depletion zone volume is significant when two cylinders are separated apart (Figure 5C). Just like the depletion attraction between cylinders that results from the tendency to


https://doi.org/10.1021/acs.macromol.4c03070
Macromolecules 2025, 58, 8099−8106

minimize the depletion zone around the cylinder body, repulsion arises while minimizing the excess depletion zone above the cylinders ($z > h$) surrounded by the overgrown polymer segments (the yellow arrows, Figure 5D), and it partially offsets the depletion attraction (the red arrows, Figure 5D) acting on the main body of the cylinders ($z < h$).

The AO theory incorporating the blob concept and depletion zone volume offers a conceptual framework for interpreting our simulation data. To further clarify the applicability of the AO theory, we have examined clustering of cylindrical inclusions driven by brush-induced depletion interactions. It is worth noting that as is most obvious for simple crowders (e.g., hard spheres), entropic forces such as depletion forces are generally nonpairwise additive.[30,32] Many-body interactions among cylinders and the correlations between brush polymers are not properly taken into account if one were to perform a simulation that employs a PMF between two cylinders without explicitly modeling brushes. For the brush-induced depletion interaction discussed here, it is evident from the geometry that if the ratio between the depletion layer thickness and the cylinder diameter ($\delta_c/D$) exceeds ≈8% ($(\delta_c/D)^* = \sqrt{3}/3 - 1/2 \approx 0.08$), the volume of the depletion zone shared by three cylinders can no longer be represented as a sum of pairwise overlaps between their individual depletion zones (see Figure 6A).[30]

Figure 6B shows the distributions of cluster size, $P(c)$, where the cluster size $c$ is defined as the number of cylindrical inclusions in a cluster, obtained from two distinct simulations (see SI for the details): (i) An implicit simulation of cylinders (circular disks) with an area fraction $\phi_c = 0.2$ without explicit brushes that employs the pairwise PMF obtained through the umbrella sampling in brushes with $N = 20$ and $\sigma b^2 = 0.06$; (ii) Brute-force MD simulation of cylinders ($\phi_c = 0.2$) inserted to an explicit brush environment ($N = 20$) at $\sigma b^2 = 0.06$. In both cases, we have chosen $D = 7.07 \times 2b$ and $h \simeq 28b$ for the cylinders. Also included are the snapshots of clusters obtained from the implicit (top) and explicit simulations of cylinders in brushes (bottom). The depletion layer thickness around the cylinders in brushes with $\sigma b^2 = 0.06$, which can be estimated directly from the inset of Figure 2B, is less than the crossover value, $\delta_c/D \approx 0.07 < (\delta_c/D)^*$. Thus, the implicit and explicit models are expected to be in agreement (Figure 6A top). At least, for $c \lesssim 10$, the implicit and explicit simulations give rise to comparable cluster size distributions. For $c > 10$, on the other hand, the explicit simulations tend to produce clusters of greater size although such a probability is relatively small (see also the inset of Figure 6B that plots the $P(c)$ in a logarithmic scale and compare the snapshots). This points to the critical role of many-body correlations, which can be incorporated to improve the current AO framework.

The results from our analysis of brush-induced depletion interactions are recapitulated as follows. The AO theory, which relies solely on the entropy argument, i.e., the principle of minimizing the depletion zone around cylindrical objects in brushes, thereby maximizing the volume for brush polymers to explore, elucidates the origin of nonmonotonic variation of depletion interactions with growing brush height. Even when the cylinder is needle-like, the depletion layer thickness is not comparable to the diameter of the cylinder as has been assumed in a previous study on bundle formation of rod-like filaments in a polymer solution[56] based on small-spherical inclusions in a semidilute solution.[47,54,55] Specifically, de Vries studied the "insertion free energy" of a thin cylinder in a polymer solution by considering the cylinder as a linear succession of small spheres of size $R_c < \xi$ and assuming that the depletion layer thickness around the cylinder remains identical to $R_c$.[56] However, in addition to Figure 2B that shows the scalings of $\delta_c \sim \sigma^{-1/2}$ for both thin and thick cylindrical inclusions, explicit calculations of $\delta_c$ around cylinders with various $D$ based on SCFT clearly show significant variation in the depletion layer thickness, especially, when $D$ is small (see Figure 7). For $D = 0.05R_0$, the $\delta_c/D$ increases steeply from $\delta_c/D \sim 0.5$ with a growing size of cylinder ($h$) and saturates to $\delta_c/D \lesssim 2$ when $h \gtrsim R_0$. This implies that in clear contradiction to the de Vries' earlier presumption, the depletion layer thickness surrounding an inclusion increases as one connects small spheres into a cylinder. These findings can be understood based on the following physical picture: a thin cylinder starts to feel the entirety of blobs if its height gets greater than the blob size ($D < \xi < h$). The blob concept is still relevant in accounting for the depletion interaction between rod-like objects in polymer solutions. As a result, the concept of correlation blobs incorporated into the AO theory as the fundamental unit of depletion interactions still proves effective in quantitative characterization of the depletion layer and stability between two inclusions, making the problem of brush-induced depletion interaction distinct from that of colloid–polymer mixtures.

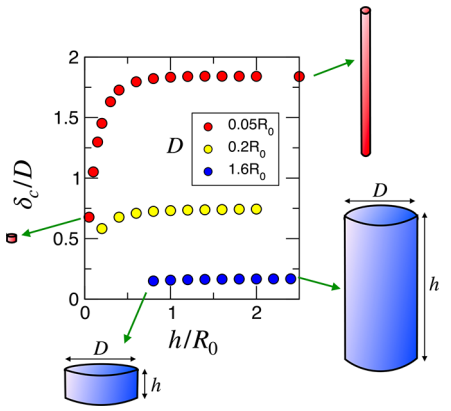


**Figure 7.** Depletion layer thickness ($\delta_c$) around cylindrical inclusions versus their height ($h$). The SCFT calculations with the excluded volume parameter $\Lambda = 2\pi^2$ were carried out (see SI) to obtain the density profile around cylinders ($\phi(\mathbf{r})$ in eq S9 in SI, and $\phi(\mathbf{r}) = c(r;z)$ due to radial symmetry around cylinders) for different aspect ratios of the cylinder. The value of $\delta_c$ was then calculated using eq 5 at the brush height, $z(<h)$, giving rise to the maximum density profile. For thin cylinders (red circles, $D = 0.05R_0$), the reduced thickness ($\delta_c/D$) initially increases rapidly with $h/R_0$ until it reaches a plateau.

## METHODS

The cylinders with $D = 3\sqrt{2}b$, $10\sqrt{2}b$, and $h = 20\sqrt{2}b$ were modeled using a composite body. The beads at the bottom layer ($z = 0.0$) were harmonically restrained along the $z$-direction with a force constant $k \simeq 10^3\epsilon/b^2$, where $\epsilon$ is the energy scale of WCA potential described below. The brush polymers were modeled by employing the potential along the chain, $U_{\text{poly}}(r_{i,i+1}) = -(k_F r_o^2/2)\ln[1 - (r_{i,i+1}/r_o)^2] + 4\epsilon[(b/r_{i,i+1})^{12} - (b/r_{i,i+1})^6 + 1/4]$ with $k_F = 30.0\epsilon/b^2$ and $r_o = 1.5b$. The monomers comprising the brush polymers and cylinders repel through the Weeks-Chandler-Andersen (WCA) potential $U_{\text{WCA}}(r) = 4\epsilon[(b/r)^{12} - (b/r)^6 + 1/4]$ for $0 < r < 2^{1/6}b$ and $U_{\text{WCA}}(r) = 0$ otherwise. To prevent polymers from penetrating the surface at $z = 0$, the WCA potential was imposed at $z = -b$. For a given $\sigma$, $n_p$ chains


https://doi.org/10.1021/acs.macromol.4c03070
Macromolecules 2025, 58, 8099−8106

were grafted to the box that has a dimension of $L_x \times L_y$ ($L_x = L_y = \sqrt{n_p/\sigma} = 100b$) with the periodic boundary imposed along the $x$ and $y$ directions. Along the $z$ direction, the shrink-wrapped boundary condition was used. Two distinct sizes of brush polymer, $N = 50$ and 150, were employed to simulate the regimes of (i), (iii) ($H < h$) and (ii), (iv) ($H > h$) in Figure 1, respectively.

The Large-scale Atomic/Molecular Massively Parallel Simulator (LAMMPS)[57] was used for the MD simulations. To calculate the PMF between the cylinders, the umbrella sampling was performed at the temperature $T = 1.0\ \epsilon/k_B$, with $k_B$ the Boltzmann constant. At each sampling point, the system was first relaxed for $10^3\tau_{MD}$ where $\tau_{MD} \approx (mb^2/\epsilon)^{1/2}$ denotes the intrinsic time scale for MD simulations, followed by a production run for $10^5\tau_{MD}$ under a bias potential, $U_b(d;d_j) = k_b(d - d_j)^2/2$, with $k_b = 200.0\ \epsilon/b^2$ and $d_j = D + 10b - jb/4$ ($j = 1, \cdots, 42$). The unbiased free energy profile was reconstructed through the weighted histogram analysis method (WHAM).[58]

## ■ ASSOCIATED CONTENT

### Supporting Information

The Supporting Information is available free of charge at https://pubs.acs.org/doi/10.1021/acs.macromol.4c03070.

Derivation of the excess area $A_{ex}(d;\delta_c)$ in eq 2; Self-consistent field calculation; Implicit vs explicit brush model (PDF)

## ■ AUTHOR INFORMATION


### Corresponding Authors

**Bae-Yeun Ha** − *Department of Physics and Astronomy, University of Waterloo, Waterloo, Ontario N2L 3G1, Canada;* orcid.org/0000-0003-2089-6759; Email: byha@uwaterloo.ca

**Changbong Hyeon** − *Korea Institute for Advanced Study, Seoul 02455, Korea;* orcid.org/0000-0002-4844-7237; Email: hyeoncb@kias.re.kr

### Authors

**Ji Woong Yu** − *Korea Institute for Advanced Study, Seoul 02455, Korea;* orcid.org/0000-0001-8479-401X

**Daeseong Yong** − *Korea Institute for Advanced Study, Seoul 02455, Korea;* orcid.org/0000-0001-6360-6622

Complete contact information is available at: https://pubs.acs.org/10.1021/acs.macromol.4c03070


### Notes

The authors declare no competing financial interest.

## ■ ACKNOWLEDGMENTS

This study was supported by the KIAS individual grants, AP091501 (J.W.Y.) and CG035003 (C.H.), the National Research Foundation of Korea (NRF) grant, NRF-2022R1C1C2010613 (D.Y.), funded by the Korea government (MSIT), and by Natural Sciences and Engineering Research Council of Canada (B.-Y.H.). We thank the Center for Advanced Computation in KIAS for providing the computing resources.

## ■ REFERENCES


(1) Aivaliotis, M.; Samolis, P.; Neofotistou, E.; Remigy, H.; Rizos, A. K.; Tsiotis, G. Molecular size determination of a membrane protein in surfactants by light scattering. *Biochimica et Biophysica Acta (BBA)-Biomembranes* **2003**, *1615*, 69−76.

(2) Lang, T.; Rizzoli, S. O. Membrane protein clusters at nanoscale resolution: more than pretty pictures. *Physiology* **2010**, *25*, 116−124.

(3) Baumgart, F.; Arnold, A. M.; Leskovar, K.; Staszek, K.; Fölser, M.; Weghuber, J.; Stockinger, H.; Schütz, G. J. Varying label density allows artifact-free analysis of membrane-protein nanoclusters. *Nat. Methods* **2016**, *13*, 661−664.

(4) Lukeš, T.; Glatzová, D.; Kvíčalová, Z.; Levet, F.; Benda, A.; Letschert, S.; Sauer, M.; Brdička, T.; Lasser, T.; Cebecauer, M. Quantifying protein densities on cell membranes using super-resolution optical fluctuation imaging. *Nat. Commun.* **2017**, *8*, 1731.

(5) Sieber, J. J.; Willig, K. I.; Heintzmann, R.; Hell, S. W.; Lang, T. The SNARE motif is essential for the formation of syntaxin clusters in the plasma membrane. *Biophys. J.* **2006**, *90*, 2843−2851.

(6) Henderson, R.; Unwin, P. N. T. Three-dimensional model of purple membrane obtained by electron microscopy. *Nature* **1975**, *257*, 28−32.

(7) Klyszejko, A. L.; Shastri, S.; Mari, S. A.; Grubmüller, H.; Muller, D. J.; Glaubitz, C. Folding and assembly of proteorhodopsin. *J. Mol. Biol.* **2008**, *376*, 35−41.

(8) Sapra, K. T.; Besir, H.; Oesterhelt, D.; Muller, D. J. Characterizing molecular interactions in different bacteriorhodopsin assemblies by single-molecule force spectroscopy. *J. Mol. Biol.* **2006**, *355*, 640−650.

(9) Hussain, S.; Kinnebrew, M.; Schonenbach, N. S.; Aye, E.; Han, S. Functional consequences of the oligomeric assembly of proteorhodopsin. *J. Mol. Biol.* **2015**, *427*, 1278−1290.

(10) Morizumi, T.; Ou, W.-L.; Van Eps, N.; Inoue, K.; Kandori, H.; Brown, L. S.; Ernst, O. P. X-ray crystallographic structure and oligomerization of Gloeobacter rhodopsin. *Sci. Rep.* **2019**, *9*, 11283.

(11) Offeddu, G. S.; Hajal, C.; Foley, C. R.; Wan, Z.; Ibrahim, L.; Coughlin, M. F.; Kamm, R. D. The cancer glycocalyx mediates intravascular adhesion and extravasation during metastatic dissemination. *Commun. Biol.* **2021**, *4*, 255.

(12) Kanyo, N.; Kovacs, K. D.; Saftics, A.; Szekacs, I.; Peter, B.; Santa-Maria, A. R.; Walter, F. R.; Dér, A.; Deli, M. A.; Horvath, R. Glycocalyx regulates the strength and kinetics of cancer cell adhesion revealed by biophysical models based on high resolution label-free optical data. *Sci. Rep.* **2020**, *10*, 22422.

(13) Buffone, A., Jr; Weaver, V. M. Don't sugarcoat it: How glycocalyx composition influences cancer progression. *J. Cell. Biol.* **2019**, *219*, No. e201910070.

(14) Shurer, C. R.; Kuo, J. C.-H.; Roberts, L. M.; Gandhi, J. G.; Colville, M. J.; Enoki, T. A.; Pan, H.; Su, J.; Noble, J. M.; Hollander, M. J.; et al. Physical principles of membrane shape regulation by the glycocalyx. *Cell* **2019**, *177*, 1757−1770.

(15) Paszek, M. J.; et al. The cancer glycocalyx mechanically primes integrin-mediated growth and survival. *Nature* **2014**, *511*, 319.

(16) Tom, A. M.; Kim, W. K.; Hyeon, C. Polymer brush-induced depletion interactions and clustering of membrane proteins. *J. Chem. Phys.* **2021**, *154*, 214901.

(17) Spencer, R. K.; Ha, B.-Y. How a Polymer Brush Interacts with Inclusions and Alters Their Interaction. *Macromolecules* **2021**, *54*, 1304−1313.

(18) Goulian, M.; Bruinsma, R.; Pincus, P. A. Long-range forces in heterogeneous fluid membranes. *Europhys. Lett.* **1993**, *22*, 145.

(19) Park, J.-M.; Lubensky, T. Interactions between membrane inclusions on fluctuating membranes. *J. Phys. (Paris)* **1996**, *7*, 1217−1235.

(20) Machta, B. B.; Veatch, S. L.; Sethna, J. P. Critical Casimir Forces in Cellular Membranes. *Phys. Rev. Lett.* **2012**, *109*, No. 138101.

(21) Spreng, B.; Berthoumieux, H.; Lambrecht, A.; Bitbol, A.-F.; Neto, P. M.; Reynaud, S. Universal Casimir attraction between filaments at the cell scale. *New J. Phys.* **2024**, *26*, No. 013009.

(22) Ben-Tal, N.; Honig, B. Helix-helix interactions in lipid bilayers. *Biophys. J.* **1996**, *71*, 3046−3050.

(23) Schmidt, U.; Guigas, G.; Weiss, M. Cluster formation of transmembrane proteins due to hydrophobic mismatching. *Phys. Rev. Lett.* **2008**, *101*, No. 128104.

(24) West, B.; Brown, F. L.; Schmid, F. Membrane-protein interactions in a generic coarse-grained model for lipid bilayers. *Biophys. J.* **2009**, *96*, 101−115.

(25) Milovanovic, D.; Honigmann, A.; Koike, S.; Göttfert, F.; Pähler, G.; Junius, M.; Müllar, S.; Diederichsen, U.; Janshoff, A.; Grubmüller, H.; Risselada, H. J.; Eggeling, C.; Hell, S. W.; van den Bogaart, G.; Jahn, R. Hydrophobic mismatch sorts SNARE proteins into distinct membrane domains. *Nat. Commun.* **2015**, *6*, 5984.
(26) Reynwar, B. J.; Illya, G.; Harmandaris, V. A.; Müller, M. M.; Kremer, K.; Deserno, M. Aggregation and vesiculation of membrane proteins by curvature-mediated interactions. *Nature* **2007**, *447*, 461−464.
(27) McMahon, H. T.; Gallop, J. L. Membrane curvature and mechanisms of dynamic cell membrane remodelling. *Nature* **2005**, *438*, 590−596.
(28) Asakura, S.; Oosawa, F. On interaction between two bodies immersed in a solution of macromolecules. *J. Chem. Phys.* **1954**, *22*, 1255−1256.
(29) Asakura, S.; Oosawa, F. Interaction between Particles Suspended in Solutions of Macromolecules. *J. Polym. Sci.* **1958**, *33*, 183−192.
(30) Lekkerkerker, H. N. W.; Tuinier, R.; Vis, M. *Colloids and the Depletion Interaction*; Springer Nature, 2024.
(31) Miyazaki, K.; Schweizer, K.; Thirumalai, D.; Tuinier, R.; Zaccarelli, E. The Asakura−Oosawa theory: Entropic forces in physics, biology, and soft matter. *J. Chem. Phys.* **2022**, *156*, No. 080401.
(32) Kang, H.; Pincus, P. A.; Hyeon, C.; Thirumalai, D. Effects of Macromolecular Crowding on the Collapse of Biopolymers. *Phys. Rev. Lett.* **2015**, *114*, No. 068303.
(33) Kang, H.; Toan, N. M.; Hyeon, C.; Thirumalai, D. Unexpected Swelling of Stiff DNA in a Polydisperse Crowded Environment. *J. Am. Chem. Soc.* **2015**, *137*, 10970−10978.
(34) Vrij, A. Polymers at interfaces and the interactions in colloidal dispersions. *Pure Appl. Chem.* **1976**, *48*, 471−483.
(35) Joanny, J.; Leibler, L.; de Gennes, P. G. Effects of polymer solutions on colloid stability. *J. Polym. Sci., Part B: Polym. Phys.* **1979**, *17*, 1073−1084.
(36) De Hek, H.; Vrij, A. Interactions in mixtures of colloidal silica spheres and polystyrene molecules in cyclohexane: I. *Phase separations. J. Colloid. interface Sci.* **1981**, *84*, 409−422.
(37) Shaw, M. R.; Thirumalai, D. Free polymer in a colloidal solution. *Phys. Rev. A* **1991**, *44*, R4797.
(38) Mao, Y.; Cates, M.; Lekkerkerker, H. N. W. Depletion force in colloidal systems. *Physica A: Statistical Mechanics and its Applications* **1995**, *222*, 10−24.
(39) Mao, Y.; Cates, M.; Lekkerkerker, H. N. W. Depletion stabilization by semidilute rods. *Phys. Rev. Lett.* **1995**, *75*, 4548.
(40) Biben, T.; Bladon, P.; Frenkel, D. Depletion effects in binary hard-sphere fluids. *J. Phys.: Condensed Matter* **1996**, *8*, 10799.
(41) Mao, Y.; Cates, M.; Lekkerkerker, H. N. W. Theory of the depletion force due to rodlike polymers. *J. Chem. Phys.* **1997**, *106*, 3721−3729.
(42) Hanke, A.; Eisenriegler, E.; Dietrich, S. Polymer depletion effects near mesoscopic particles. *Phys. Rev. E* **1999**, *59*, 6853.
(43) Aarts, D.; Tuinier, R.; Lekkerkerker, H. N. W. Phase behaviour of mixtures of colloidal spheres and excluded-volume polymer chains. *J. Phys.: Condensed Matter* **2002**, *14*, 7551.
(44) Marrenduzzo, D.; Finan, K.; Cook, P. R. The depletion attraction an underappreciated force driving cellular organization. *J. Cell. Biol.* **2006**, *175*, 681−686.
(45) Binder, K.; Virnau, P.; Statt, A. Perspective: The Asakura Oosawa model: A colloid prototype for bulk and interfacial phase behavior. *J. Chem. Phys.* **2014**, *141*, 559.
(46) Eisenriegler, E. Universal density-force relations for polymers near a repulsive wall. *Phys. Rev. E* **1997**, *55*, 3116.
(47) de Gennes, P. G. Suspensions colloïdales dans une solution de polymères. *C. R. Acad. Sci. B* **1979**, *288*, 359−361.
(48) Eisenriegler, E. Polymers interacting with mesoscopic particles. *J. Phys.: Condens. Matter* **2000**, *12*, A227.
(49) de Gennes, P. G. *Scaling Concepts in Polymer Physics*; Cornell University Press: Ithaca and London, 1979.
(50) Alexander, S. Adsorption of chain molecules with a polar head a scaling description. *J. Phys. (Paris)* **1977**, *38*, 983−987.
(51) de Gennes, P. G. Conformations of polymers attached to an interface. *Macromolecules* **1980**, *13*, 1069−1075.
(52) de Gennes, P. G. Polymers at an interface; a simplified view. *Adv. Colloid Interface Sci.* **1987**, *27*, 189−209.
(53) Hansen, P. L.; Cohen, J. A.; Podgornik, R.; Parsegian, V. A. Osmotic properties of poly (ethylene glycols): quantitative features of brush and bulk scaling laws. *Biophys. J.* **2003**, *84*, 350−355.
(54) Odijk, T. Protein-Macromolecule Interactions. *Macromolecules* **1996**, *29*, 1842−1843.
(55) Sear, R. P. Entropy-driven phase separation in mixtures of small colloidal particles and semidilute polymers. *Phys. Rev. E* **1997**, *56*, 4463.
(56) de Vries, R. Flexible polymer-induced condensation and bundle formation of DNA and F-actin filaments. *Biophys. J.* **2001**, *80*, 1186−1194.
(57) Thompson, A. P.; Aktulga, H. M.; Berger, R.; Bolintineanu, D. S.; Brown, W. M.; Crozier, P. S.; In't Veld, P. J.; Kohlmeyer, A.; Moore, S. G.; Nguyen, T. D.; et al. LAMMPS-a flexible simulation tool for particle-based materials modeling at the atomic, meso, and continuum scales. *Comput. Phys. Commun.* **2022**, *271*, No. 108171.
(58) Kumar, S.; Bouzida, D.; Swendsen, R. H.; Kollman, P. A.; Rosenberg, J. M. The weighted histogram analysis method for free-energy calculation on biomolecules. *I. The method. J. Comp. Chem.* **1992**, *13*, 1011−1021.




https://doi.org/10.1021/acs.macromol.4c03070
*Macromolecules* 2025, 58, 8099−8106